Acta Pharmacologica Sinica (2017) 38: 931–942
 1671-4083/17
www.nature.com/aps

Original Article

A versatile nanoplatform for synergistic combination therapy to treat human esophageal cancer

Xin-shuai WANG[1], De-jiu KONG[1], Tzu-yin LIN[2], Xiao-cen LI[4], Yoshihiro IZUMIYA[3], Xue-zhen DING[1], Li ZHANG[1], Xiao-chen HU[1], Jun-qiang YANG[1], She-gan GAO[1], Kit S LAM[4], Yuan-pei LI[4, *]

[1]Henan Key Laboratory of Cancer Epigenetics; Cancer Hospital, The First Affiliated Hospital, College of Clinical Medicine, Medical College of Henan University of Science and Technology, Luoyang 471003, China; [2]Department of Internal Medicine, Division of Hematology/Oncology, University of California Davis, Sacramento, CA 95817, USA; [3]Department of Dermatology, University of California Davis, Sacramento, CA 95817, USA; [4]Department of Biochemistry & Molecular Medicine, UC Davis Comprehensive Cancer Center, University of California Davis, Sacramento, CA 95817, USA

Abstract

One of the major goals of precision oncology is to promote combination therapy to improve efficacy and reduce side effects of anti-cancer drugs based on their molecular mechanisms. In this study, we aimed to develop and validate new nanoformulations of docetaxel (DTX) and bortezomib (BTZ) for targeted combination therapy to treat human esophageal cancer. By leveraging our versatile disulfide cross-linked micelles (DCMs) platform, we developed nanoformulations of DTX and BTZ (named DTX-DCMs and BTZ-DCMs). Their physical properties were characterized; their anti-cancer efficacies and mechanisms of action were investigated in a human esophageal cancer cell line *in vitro*. Furthermore, the *in vitro* anti-tumor activities of combination therapies (concurrent drug treatment, sequential drug treatment, and treatment using different ratios of the drugs) were examined in comparison with the single drug treatment and free drug strategies. These drug-loaded nanoparticles were spherical in shape and relatively small in size of approximately 20–22 nm. The entrapment efficiencies of DTX and BTZ into nanoparticles were 82.4% and 84.1%, respectively. The drug release rates of DTX-DCMs and BTZ-DCMs were sustained, and greatly increased in the presence of GSH. These nanodrugs were effectively internalized by KYSE30 esophageal cancer cells, and dose-dependently induced cell apoptosis. We further revealed a strong synergistic effect between DTX-DCMs and BTZ-DCMs against KYSE30 esophageal cancer cells. Sequential combination therapy with DTX-DCMs followed by BTZ-DCMs exhibited the best anti-tumor efficacy *in vitro*. This study demonstrates that DTX and BTZ could be successfully nanoformulated into disulfide cross-linked micelles. The nanoformulations of DTX and BTZ demonstrate an immense potential for synergistic combination therapy to treat human esophageal cancer.

Keywords: nanoformulations; disulfide cross-linked micelles; docetaxel; bortezomib; targeted combination therapy; synergistic effect; human esophageal cancer

Acta Pharmacologica Sinica (2017) 38: 931–942; doi: 10.1038/aps.2017.43; published online 22 May 2017

Introduction

Esophageal cancer is one of the most common malignant tumors worldwide. Global cancer statistical data[1] estimate that there are 456 000 new cases of esophageal cancer in the world, accounting for 3.2% of all malignant tumors that were diagnosed in 2012. In China, esophageal cancer cases account for approximately 50% of all new cases worldwide. Chinese esophageal cancer has killed 197 500 people, accounting for 49.35% of the global total. In China, the current death totals due to esophageal cancer rank fourth out of all malignant tumors[2].

Precision medicine is an emerging approach to disease treatment and prevention that considers the variability in an individual's environment, lifestyle and genetics. The short-term goals involve expanding precision medicine into cancer research. Testing combinations of targeted agents to identify approaches to improve their efficacy and to overcome drug resistance is a major emphasis of precision oncology[3].

Docetaxel (DTX), a semi-synthetic analog of paclitaxel (PTX), can prevent physiological microtubule depolymerization, resulting in cell cycle arrest in the G_2/M phases and cell death in cancer cells[4]. It has proven effective in a range of tumors[5–9], such as breast cancer, ovarian cancer, non-small-cell lung cancer, gastric carcinomas and esophageal cancer.

*To whom correspondence should be addressed.
E-mail lypli@ucdavis.edu
Received 2016-12-11 Accepted 2017-03-23

DTX promotes the expression of the cell cycle inhibitor p27 and inhibits expression of the antiapoptotic gene Bcl-2[10, 11]. Bortezomib (BTZ, Velcade®), a selective and potent inhibitor of the proteasome, promotes apoptosis via the stabilization of p53, p21, p27, and IkappaB-alpha, resulting in nuclear factor kappaB inhibition[12]. BTZ has also been shown to overcome Bcl-2-mediated protection from apoptosis[13]. BTZ combined with DTX exhibited excellent activity in preclinical models of human solid tumors, especially in pancreatic cancer, NSCLC, head and neck squamous cell carcinoma (HNSCC), prostate cancer, gastroesophageal junction (GEJ) and gastric adenocarcinoma[14–18]. Combination therapy also reduced tumor microvessel densities, which was related to tumor cell production of the vascular endothelial growth factor and increased levels of apoptosis in tumor-associated endothelial cells[15]. In addition, a California cancer consortium trial for NSCLC confirmed that DTX plus BTZ given either sequentially or concurrently have similar response rates (RR) and progression-free survivals (PFS). The median survival in the sequential arm exceeded published survival estimates for either agent alone or in combination[18]. Moreover, preclinical studies in prostate and lung cancer models indicated that sequential DTX-BTZ treatment was more effective than BTZ-DTX treatment[19]. The explicable mechanism for this phenomenon may be that BTZ promotes cell cycle arrest before the M phase, which then interferes with DTX-induced apoptosis[15]. The knowledge gained from clinical practice regarding the interactions of these two agents has great implications for improving esophageal cancer therapy.

Although it appears promising, the application of this combination therapy is restricted due to the poor solubility, low selective distribution and fast elimination of the drugs. Furthermore, it has been reported to cause severe systemic toxicity, including bone marrow suppression, musculoskeletal toxicity, peripheral neuropathy and hypersensitivity reactions attributable to either the drug itself or the solvent system[20–23]. The toxicity remarkably limited the intensity of chemotherapy and lessened the quality of life for the patients.

To successfully address these issues, several formulation approaches have been attempted to enhance the physicochemical properties, such as using nanoparticles, liquid self-nanoemulsifying drug delivery systems (SNEDDS)[24] and pretreatment with P-glycoprotein inhibitors[25]. Nanoparticle formulation can deliver drugs specifically to tumor sites while sparing normal tissues to increase the therapeutic index. We have demonstrated that reversible disulfide cross-linked micelles (DCMs)[26] could minimize the premature release of drugs from carriers while they are circulating in the blood stream. Cross-linking not only improved the structural stability of micelles but also controlled the release rates of the entrapped drugs[27]. It was also demonstrated that the disulfide cross-linked micellar formulation of PTX (PTX-DCMs) was more efficacious than both free drugs and the non-cross-linked formulation of PTX at equivalent doses of PTX in the ovarian cancer xenograft mouse model[28]. Taking advantage of this unique nanoplatform, we aimed to develop nanoformulations of DTX and BTZ by encapsulating them into DCMs, which are formed by the self-assembly of telodendrimers (PEG^{5k}-Cys_4-L_8-CA_8). Thus, the delivery of DTX-DCMs and BTZ-DCMs could be accomplished by a passive process, which refers to particle transportations into tumor cells and the interstitium by passive diffusion and convection[29]. A selective accumulation of particles that contain DTX and BTZ could be achieved through enhanced permeability and retention (EPR) effects *in vivo*.

In this study, we have presented the development and validation of a new nanoformulation of DTX and BTZ for esophageal cancer treatment. The drug loading efficiency, size and morphology of these nanoformulations were characterized by high-performance liquid chromatography (HPLC), dynamic light scattering (DLS) and transmission electron microscopy (TEM), respectively. The drug release was investigated by the dialysis method. The cellular uptake of DTX-DCMs and BTZ-DCMs was evaluated by confocal laser scanning microscopy in the human esophageal cancer cell line KYSE30. Upon treatment, cell apoptosis and cell cycle analysis were determined with flow cytometry. Potential molecular mechanisms were discovered by Western blot analysis. Finally, the *in vitro* antitumor activities of combination therapies (concurrent drug treatment, sequential drug treatment, and treatment using different ratios of the drugs) using DTX-DCMs and BTZ-DCMs were evaluated in KYSE30 cells in comparison with single treatment and free drug treatment.

Materials and methods

Materials

DTX was purchased from AK Scientific Inc (Mountain View, CA, USA). BTZ was purchased from LC Laboratories (Woburn, MA, USA). 1,1′-Dioctadecyl-3,3,3′,3′-tetramethylindodicarbocyanineperchlorate (DiD) and 4′,6-diamidino-2-phenylindole (DAPI) were purchased from Life Technologies (Grand Island, NY, USA). Human KYSE30 esophageal squamous epithelial cancer cells were obtained from the American Type Culture Collection (Rockville, MD, USA). RPMI-1640 medium was purchased from Gibco (Carlsbad, CA, USA). MTT [3-(4,5-dimethyl-diazol-2-yl)-2,5 diphenyl tetrazolium bromide] and all other chemicals were purchased from Sigma-Aldrich (St Louis, MO, USA). Anti-p-ERK, anti-PKCε, anti-p38, anti-Bcl-2 and anti-p65 were purchased from ABGENT (Santa Cruz Biotechnology, Santa Cruz, CA, USA).

Synthesis of DCM

The thiolated telodendrimer (PEG^{5k}-Cys_4-L_8-CA_8) was synthesized via solution-phase condensation reactions from MeO-PEG-NH_2 utilizing stepwise peptide chemistry[28, 30].

Preparation and characterization of DTX-DCMs and BTZ-DCMs

DTX was loaded into the micelles using the solvent evaporation method[31]. Briefly, DTX (1 mg) and PEG^{5k}-Cys_4-L_8-CA_8 telodendrimers (20 mg) were first dissolved in chloroform in a 1-mL round-bottom flask. The chloroform was evaporated under a vacuum to form a thin film. PBS buffer (1 mL) was

added to re-hydrate the thin film, followed by 20 min of sonication. The DTX-loaded micelles were then cross-linked via O^2-mediated oxidization as described above. The amount of drug loaded into the micelles was analyzed with an HPLC system (Milford, MA, USA) after the drugs were released from the micelles by adding 9× acetonitrile followed by 10 min of sonication. Drug loading was calculated according to the calibration curve between the HPLC area values and the concentrations of the drug standard. Loading capacity is defined as the highest drug concentration that can be achieved by the micelles in an aqueous solution, while loading efficiency is defined as the ratio of drug loaded into micelles to the initial drug content. Part of the DTX-loaded micelle solution was stored at 4 °C for characterization, and the rest was lyophilized[32, 33]. The preparation method for BTZ-DCMs is similar to the steps mentioned above. DiD (hydrophobic NIRF dye, 0.5 mg/mL) was loaded into the micelles either separately or together with the drugs using the same method described above. The micelle solution was filtered with a 0.22-μm filter to sterilize the sample.

The morphology, particle size distribution (diameter, nm), polydispersity index (PDI), and surface charge (zeta potential, mV) of DTX-DCMs and BTZ-DCMs were characterized by transmission electron microscopy (TEM, Philips CM-120, Amsterdam, Netherlands) and dynamic light scattering (DLS) instruments (Malvern, Zetasizer nano series Nano-ZS, Malvern, UK, respectively). The drug concentrations of DTX-DCMs and BTZ-DCMs were kept at 1.0 mg/mL for DLS measurements. All measurements were performed at 25 °C, and the data were analyzed with Zetasizer Nano Software v3.30. For TEM, the aqueous micelle solution (1 mg/mL) was deposited onto copper grids and measured at room temperature. The drug loading content (DLC) and the drug loading efficiency (DLE) of DTX-DCMs and BTZ-DCMs were calculated using the following equations: DLC (%)=$W_{\text{loaded drug}}$/$W_{\text{drug loaded DCMs}}$×100% and DLE (%)=$W_{\text{loaded drug}}$/$W_{\text{free drug}}$×100%.

Drug release study

The *in vitro* drug release profiles for the different formulations of DTX and BTZ were measured using the dialysis method. DCMs were prepared with 20 mg/mL telodendrimer and loaded with 1 mg/mL DTX and BTZ. Aliquots of the conventional formulations of DTX (1 mg/mL), BTZ (1 mg/mL), DTX-DCMs and BTZ-DCMs were injected into dialysis cartridges with a MWCO of 3.5 kDa (Thermo Scientific, Rockford, IL, USA). Cartridges were dialyzed against 1 L of PBS with shaking at 100 rpm in the presence of 10 g/L activated charcoal to create a sink condition. The concentrations of DTX and BTZ that remained in the dialysis cartridges at various time points were measured with a UV-visible spectrometer after releasing the drug from the micelles by adding 9× DMSO followed by 10 min of sonication. Values are reported as the mean for each triplicate sample.

Cell culture and cellular uptake

Cells were cultured in ATCC-formulated RPMI-1640 medium supplemented with 10% fetal bovine serum (FBS), 100 U/mL penicillin G and 100 μg/mL streptomycin at 37 °C using a humidified 5% CO_2 incubator.

For the cellular uptake study, the DiD dye was co-loaded with DTX into DCMs using a similar method that was used to generate the DTX-loaded DCMs. The KYSE30 esophageal cancer cell line was seeded at a density of 5×10^4 cells per well on eight-well tissue culture chamber slides (BD Biosciences, Bedford, MA, USA) overnight. The cells were incubated with DiD-DTX-DCMs for 4 h and washed three times with PBS. The slide was fixed with 4% paraformaldehyde, and the cell nuclei were stained with DAPI. After mounting with cover slips, the slides were observed under a confocal laser scanning microscope (Carl Zeiss, LSM 800, Zeiss, Jena, Germany).

In vitro cytotoxicity assay and optimization of the drug loading ratio

The cell viability after treatments with DTX, BTZ, BTZ-DCMs, DTX-DCMs or combination treatment was determined by the MTT assay (GraphPad Prism5.0, CA, USA)[34]. KYSE30 cells were seeded in 96-well plates at a density of 5×10^3 cells/well 24 h prior to the treatment. Cells were treated in triplicate with various concentrations of DTX, BTZ, BTZ-DCMs, DTX-DCMs or combination treatment, as indicated. After 72 h of incubation, the cultured medium was removed and fresh medium containing MTT dye (2 mg/mL) was added to each well; the plates were incubated at 37 °C for 4 h. The absorbance at 490 nm was detected using a microplate ELISA reader (SpectraMax M2, Molecular Devices, USA). Cell viability, as a percent of the untreated control, was calculated as follows: $[(OD_{\text{treat}}-OD_{\text{blank}})/(OD_{\text{control}}-OD_{\text{blank}})\times100\%]$ for triplicate wells. The combination therapy was performed by adding BTZ-DCMs and DTX-DCMs concurrently as well as sequentially. We further investigated the impact of the drug ratio on the variability of the KYSE30 cells. The pre-selected initial concentrations of DTX-DCMs/BTZ-DCMs for combination therapy were 200 μg/mL:40 μg/mL (5:1), 200 μg/mL:100 μg/mL (2:1), 200 μg/mL:200 μg/mL (1:1), 100 μg/mL:200 μg/mL (1:2), and 40 μg/mL:200 μg/mL (1:5). Then, a series of dilutions was prepared using a double dilution method, and 10 different concentrations were used for the *in vitro* cytotoxicity assay. To obtain reliable results, the experiments described above were repeated three times.

Apoptosis detection and cell cycle analysis by flow cytometry

KYSE30 cell apoptosis was assessed using Annexin V-FITC and propidium iodide (PI) double staining (Pharmingen, San Diego, CA, USA). Cells in the logarithmic growth phase were placed in a 6-well plate at a density of 1×10^6 cells per well overnight. Later, the cells were treated with 0.3, 3 and 30 μg/mL DTX-DCMs for 24 h. All cells and supernatants were collected for analysis. After centrifugation, the cells were stained with 10 μg/mL Annexin V-FITC at room temperature in the dark for 30 min. Before analysis was performed, 20 μg/mL PI was added and the samples were incubated for 5 min on ice while being protected from light. Samples were analyzed by flow

cytometry (Becton-Dickinson, Mansfield, MA, USA).

For cell cycle analysis, the cells were treated as previously described. After 24 h of drug incubation, the cells were collected and fixed with 70% alcohol containing 3% serum at 4 °C for 24 h. RNase-A (Sigma-Aldrich) was added to a final concentration of 100 μg/mL in a water bath for 30 min at 37 °C for digestion. Propidium iodide was added to a final concentration of 50 μg/mL in an ice bath for 30 min away from light for staining. After filtering with a 300-screen nylon mesh, the cells were observed by flow cytometry. The number of cells in the G_0/G_1, S and G_2/M phases was calculated with FlowJo software. Testing was performed in triplicate for each group.

Protein preparation and Western blot analysis

Several proteins that are involved in apoptosis and cell cycle regulation were analyzed by Western blot. DTX was added, followed by DTX-DCMs, after 1×10^6 cells were cultured for 24 h, and then the cells were washed with PBS and lysed in a buffer containing 20 mmol/L Tris-HCL (pH 7.6), 150 mmol/L NaCl (pH 6.85), 1 mmol/L EDTA (pH 8), 1% Triton X-100, 2.5 mmol/L sodium pyrophosphate, 1 mmol/L sodium orthovanadate (Na_3VO_4), 1 mg/mL leupeptin, 1% protease inhibitor cocktail and 1% phosphatase inhibitor cocktail (Sigma-Aldrich NV/SA, Bornem, Belgium). The lysates were centrifuged at 12000×*g* for 10 min at 4 °C and then boiled for 5 min. The protein concentration of the lysate was detected using the Bio-Rad Bradford protein assay (Nazareth Eke, Belgium), and 25 μg of denatured protein was subjected to SDS-PAGE (10% SDS-acrylamide gel) with a loading buffer that contained 80 mmol/L Tris–HCl (pH 6.8), 5% SDS, 10% glycerol, 5 mmol/L EDTA (pH 8), 5% 2-mercaptoethanol, 0.2% bromophenol blue and 1 mmol/L phenylmethylsulfonyl fluoride. The separated proteins were transferred at 100 mA to PVDF membranes (Bio-Rad) for 2 h. The membranes were incubated as indicated with the following primary antibodies: p-ERK (anti-ERK1 antibody), NF-κB (Ser536), p38 (p38 antibody), PKCε (PKCε antibody), Bcl-2 (Bcl-2 antibody) and α-tubulin (Sigma-Aldrich NV). A peroxidase-conjugated secondary antibody (1:4000 dilution, ECL Anti-mouse or Anti-rabbit IgG HRP linked, Na 931, GE Healthcare Biosciences/Amersham, Diegem, Belgium) was added. Immunoreactive bands were visualized with SuperSignal West Dura Extended Duration Substrate, which is an enhanced chemiluminescent substrate (Pierce Biotechnology, Rockford, IL, USA), and the results of electrophoresis were analyzed by Quantity One (Bio-Rad). Each experiment was performed independently at least three times.

Statistical analysis

Statistical analyses were performed using Student's *t*-test for two groups and one-way analysis of variance (ANOVA) for multiple groups. All results are expressed as the mean±standard error (SEM) unless otherwise noted. A value of $P<0.05$ was considered statistically significant.

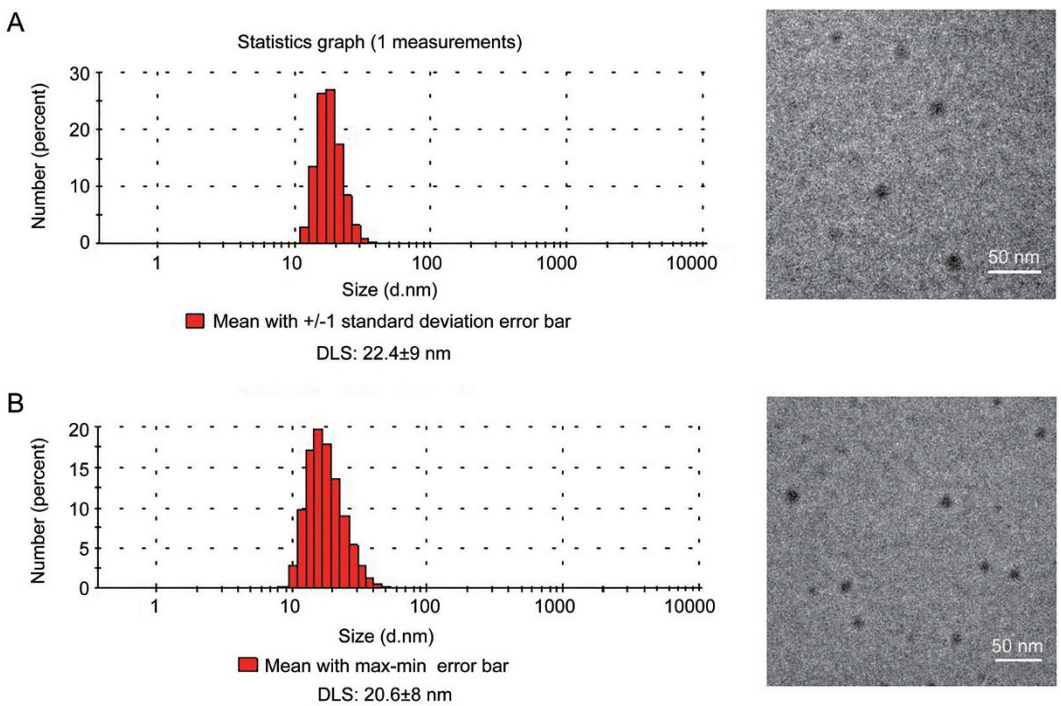

Figure 1. DLS size distribution and TEM image of DTX-DCMs (A) and BTZ-DCMs (B). (Left) The diameters of DTX-DCMs and BTZ-DCMs were 22.4±9 nm and 20.6±8 nm, respectively, as analyzed by DLS. Their PDIs were 0.18±0.06 and 0.17±0.05, respectively, and the Zeta potential results were +26.9±3.7 mV and +28.1±2.9 mV, respectively. (Right) These drug-loaded nanoparticles were uniformly sphere-shaped according to observation by TEM.

Results

Characterization of drug-DCMs

As analyzed by DLS (Figure 1, left), DTX-DCMs and BTZ-DCMs were 22.4±9 nm and 20.6±8 nm in diameter, respectively, with a narrow distribution. The PDIs of DTX-DCMs and BTZ-DCMs were 0.18±0.06 and 0.17±0.05, respectively, while their zeta potential was +26.9±3.7 mV and +28.1±2.9 mV, respectively. According to TEM observations, these drug-loaded nanoparticles were uniformly sphere shaped, and their size agreed with the DLS results. Through HPLC analysis, we determined the drug content and loading efficiency of DTX and BTZ in DCMs. The DLE of DTX in DTX-DCMs and BTZ in BTZ-DCMs was 82.4% and 84.1%, respectively, while the DLCs were 15.6% and 13.7%, respectively.

Cell uptake

Confocal laser scanning microscopy was utilized to study the intracellular delivery of DTX- and BTZ-loaded DCMs. The cellular uptake of empty and drug-loaded nanoparticles with fluorescent labeling (DiD) was investigated in KYSE30 human esophageal cancer cells after 2 h of incubation. As shown in Figure 2, DTX-DCMs and BTZ-DCMs could be effectively internalized into KYSE30 cells. In addition, confocal microscopy images demonstrated that the drug-DCMs in tumor cells were mainly located in the cytoplasmic region of KYSE30 cells after internalization (Figure 2).

Flow cytometry analysis

Cell apoptosis analysis

To characterize the apoptotic effects of the DTX-DCMs and BTZ-DCMs in relation to mitotic arrest activities, the apoptosis of KYSE30 cells at different concentrations was assessed using flow cytometry. After KYSE30 cells were exposed to drug-DCMs with different concentrations for 2 h, KYSE30 cells were analyzed by FlowJo 7.6.1 software. As shown in Figure 3, the early apoptosis rates of KYSE30 cells at different concentrations of DTX-DCMs were 0.152% (0.3 μg/mL) and 0.486% (3 μg/mL), and the late apoptosis rates were 5.79%

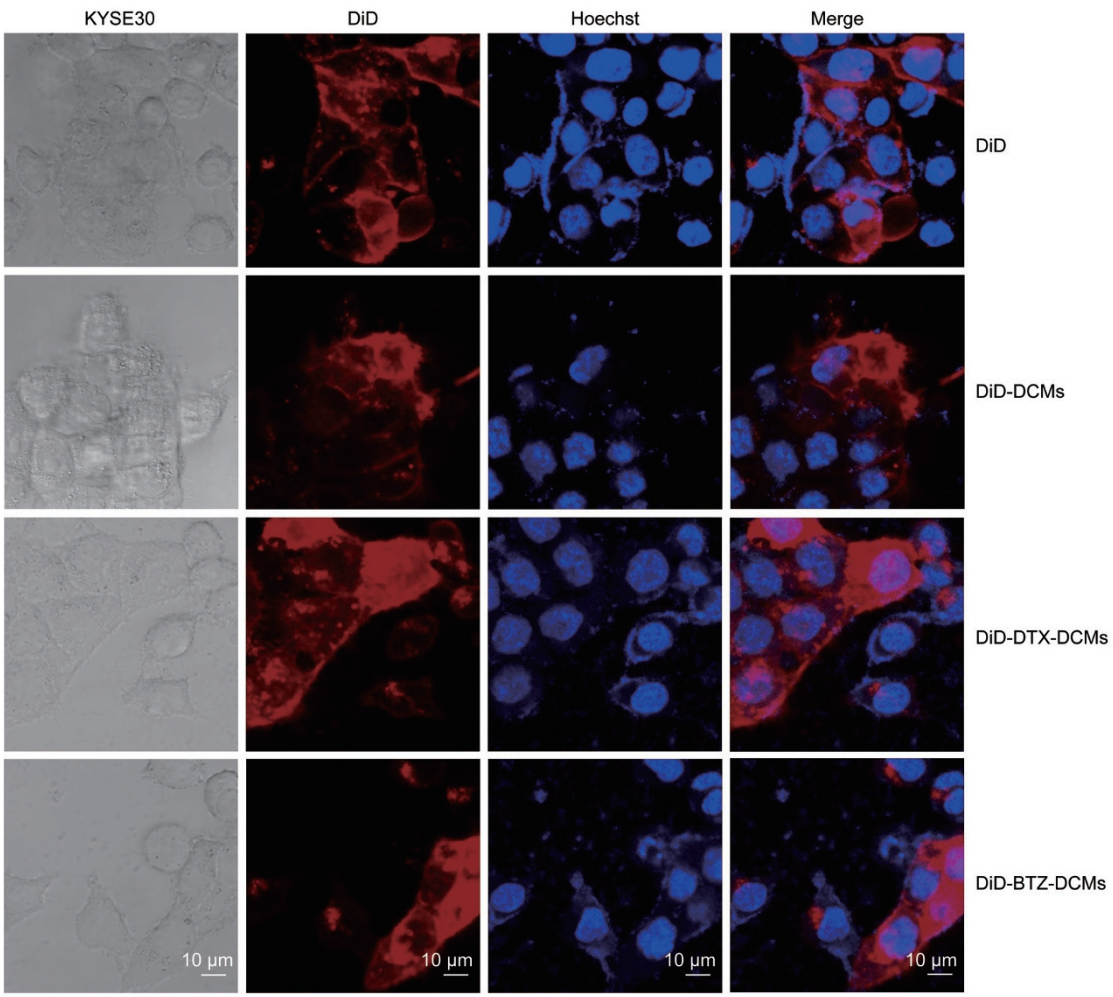

Figure 2. Intracellular delivery of DTX-DCMs and BTZ-DCMs. Uptake of free DiD, DiD-loaded DCMs and DiD/drug co-loaded DCMs (red) in KYSE30 esophageal cancer cell lines. Cells were cultured in 8-well chamber slides with cover glass overnight. Cells were pre-treated with Hoechst 33342 (blue) for 10 min for nuclear staining followed by incubation with DID in PBS. Imaging was acquired at 2 h using a confocal laser scanning microscope. Scale bar=10 μm.

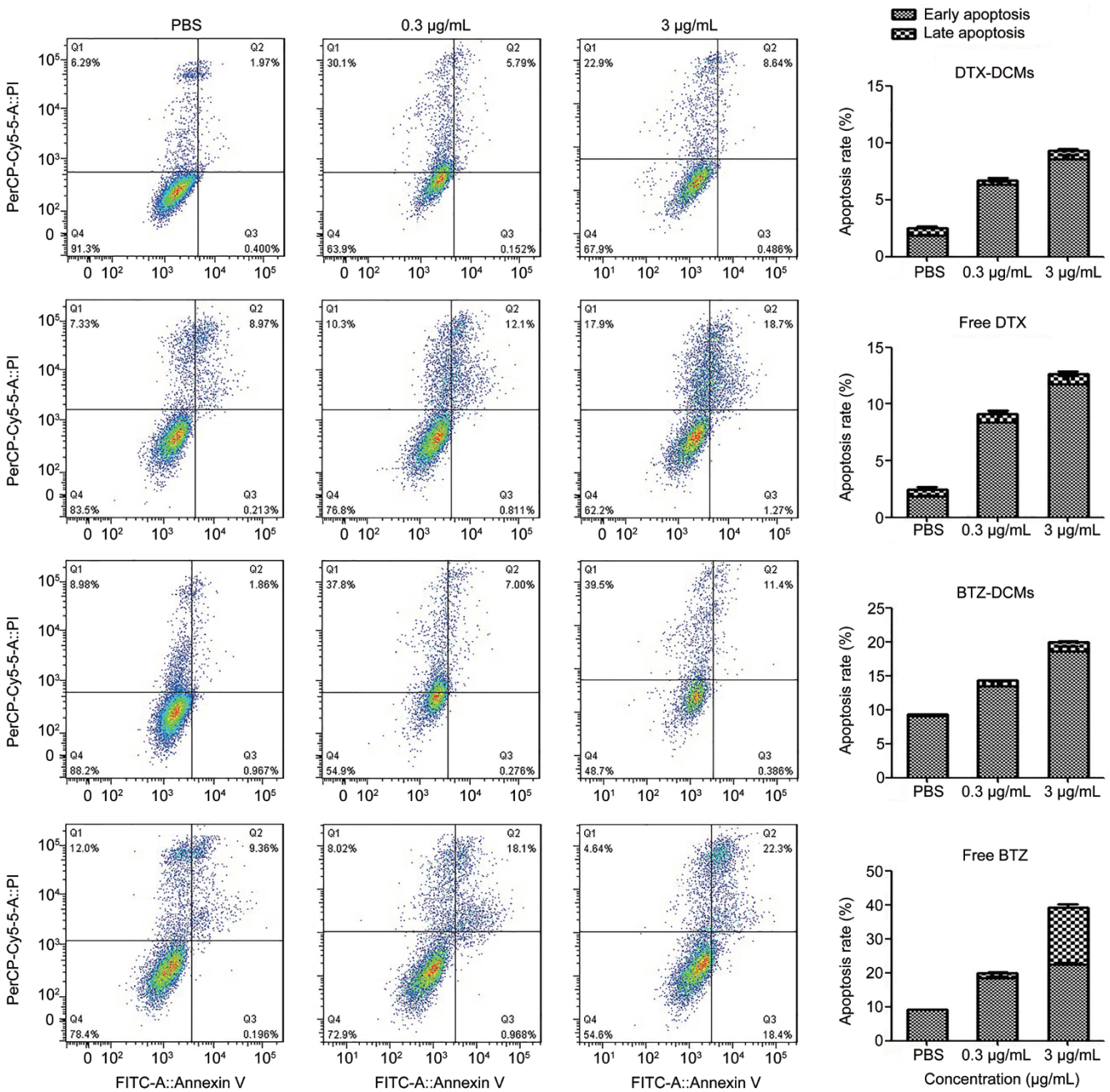

Figure 3. Cell apoptosis analysis represented as a histogram. The proportion of different cell apoptosis phases (Q1: necrotic cells; Q2: late apoptotic cells; Q3: early apoptotic cells; Q4: live cells) with different concentrations (0.3 and 3 μg/mL) of drug-DCMs and free drug are analyzed by flow cytometry. The percentage of cells in different cell apoptosis phases is expressed in the histogram, and the data are presented as the mean and SE from three independent experiments.

(0.3 μg/mL) and 8.64% (3 μg/mL). The total apoptosis rates, including early and late apoptosis, were approximately 5.94% (0.3 μg/mL) and 9.12% (3 μg/mL). In comparison to DTX-DCMs, the total apoptosis rates of DTX were approximately 12.91% (0.3 μg/mL) and 19.97% (3 μg/mL). Additionally, the early apoptosis rates of KYSE30 cells at different concentrations of BTZ-DCMs were 0.276% (0.3 μg/mL) and 0.386% (3 μg/mL), and the late apoptosis rates were 7.00% (0.3 μg/mL) and 11.4% (3 μg/mL). The total apoptosis rates, including early and late apoptosis, were approximately 7.27% (0.3 μg/mL) and 11.78% (3 μg/mL). In addition, the total apoptosis rates of BTZ were approximately 19.07% (0.3 μg/mL) and 40.70% (3 μg/mL). It was demonstrated that total apoptosis rates stably increased with increases in drug concentration.

Cell cycle analysis

The anti-cancer effect of DTX has been shown to be related

to blocked mitosis, which results in cell cycle arrest in the G_2/M phase. To investigate whether aberrant mitosis was observed in DTX-DCMs-treated KYSE30 cells, increasing concentrations (0.3, 3, and 30 μg/mL) of DTX-DCMs were used to treat KYSE30 cells following cell cycle analysis. The results obtained from the different concentrations are shown in Figure 4. DTX-DCMs caused a dose-dependent increase of G_2 phase accumulation. The percentages of G_2 phase accumulation after 0.3 and 3 μg/mL DTX-DCMs treatments were 26.92% and 35.71%, respectively. Additionally, the percentages of the G_1 phase cells decreased to 6.66% and 1.03% at the concentrations of 0.3 and 3 μg/mL DTX-DCMs, respectively. Most of the cells were dead at 30 μg/mL and the results are not shown. The results also confirmed that DTX-DCMs caused cell cycle arrest, eventually resulting in cancer cell apoptosis. As shown in Figure 4, the proportion of the differentiating stages that were treated with different concentrations of BTZ-DCMs was analogous, which illustrated that BTZ was not the drug that induced apoptosis by inhibiting differentiation. The results from DTX and BTZ were similar to that of DTX-DCMs and BTZ-DCMs (Figure 4).

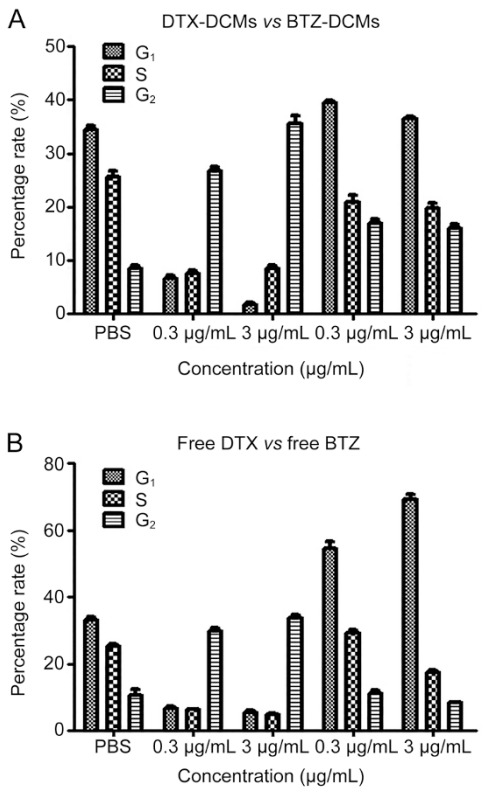

Figure 4. Cell cycle distribution represented as a histogram. Cell cycle distribution and arrest in the G_1, S and G_2 phases with different concentrations (0.3 and 3 μg/mL) of drug-DCMs and free drug were analyzed by flow cytometry. The percentage of cells in each phase is expressed in the histogram, and the data are presented as the mean and SE from three independent experiments.

Western blot analysis

Western blot was used to investigate the possible molecular mechanisms of DTX-DCMs and BTZ-DCMs against KYSE30 cells. Some factors, such as p-ERK, p65, p38, Bcl-2 and PKCε, were reported to affect the growth and proliferation of various cancers. Thus, these factors were selected to examine and explore the mechanisms of DTX-DCMs and BTZ-DCMs on KYSE30 cells in this study. The results showed that the expression levels of p-ERK, p65 and PKCε in cells after treatment with both nanodrugs were increased compared with the control group, but the levels of p38 and Bcl-2 were decreased (Figure 5). Alpha-tubulin was used as a protein loading control.

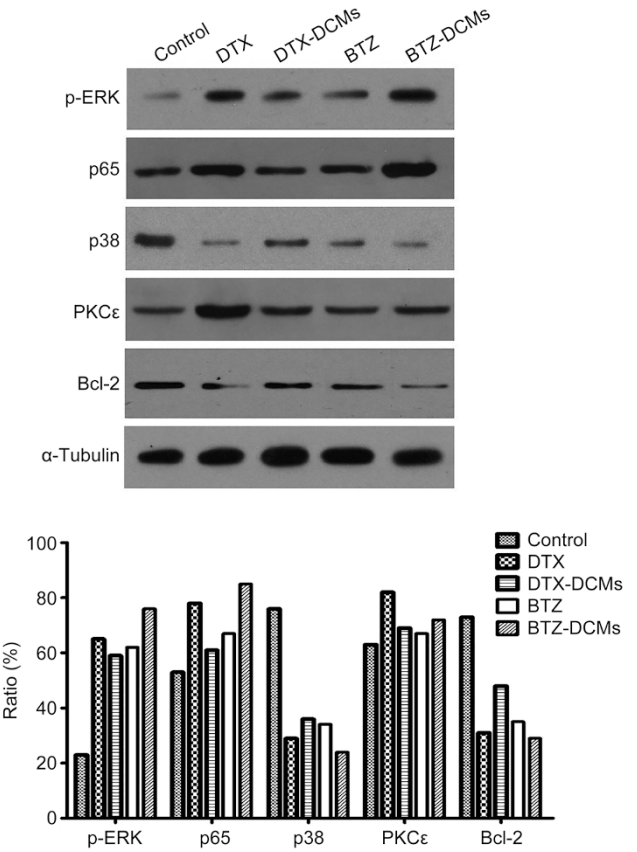

Figure 5. Western blot analysis represented as a histogram. The levels of p-ERK, p65, p38, Bcl-2 and PKCε in KYSE30 esophageal cancer cell lines treated with free DTX/DTX-DCMs and BTZ/BTZ-DCMs assayed by Western blot. α-Tubulin was used as a protein loading control.

Drug release and optimization of the drug loading ratio

As shown in Figure 6, the drug release from DTX-DCMs and BTZ-DCMs was sustained. The initial drug release rates of DTX-DCMs and BTZ-DCMs in the first 24 h was approximately 20%, and then it decreased even more. In the presence of GSH, the release rates in 24 h were greater than 40%. The

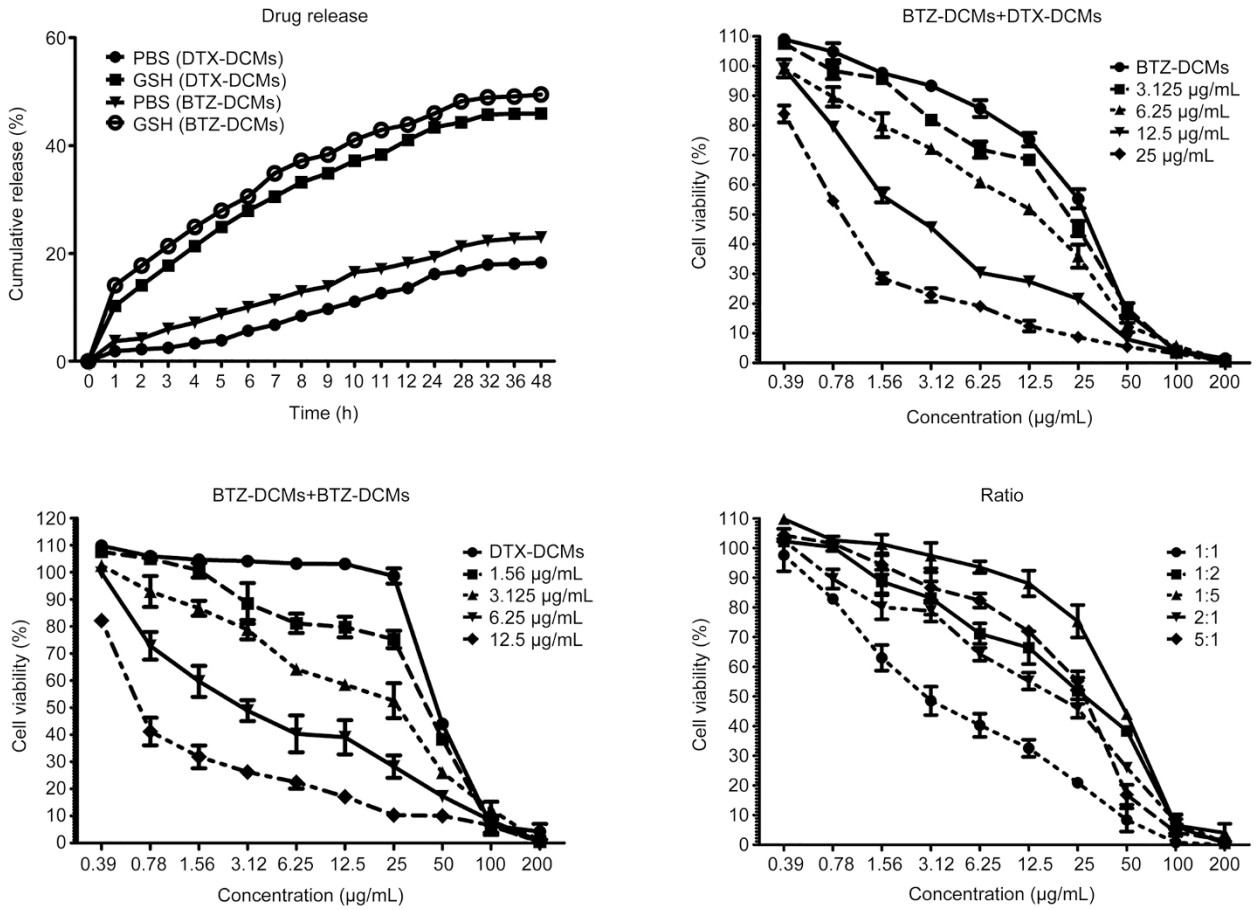

Figure 6. Drug release and optimization of the drug loading ratio. (A) The drug release curve showed the release process of drug-DCMs in PBS and GSH. (B) MTT assays showed cell viability results when DTX-DCMs were 0, 3.125, 6.25, 12.5 and 25 μg/mL with different concentrations of BTZ-DCMs. (C) MTT assays showed cell viability results when BTZ-DCMs were 0, 1.56, 3.125, 6.25 and 12.5 μg/mL with different concentrations of DTX-DCMs. (D) MTT assays showed cell viability results the when the drug loading ratios of DTX-DCMs/BTZ-DCMs were 5:1, 2:1, 1:1, 1:2, 1:5.

results show that this nanocarrier has the characteristic of a sustained release, and it could be triggered by GSH to release drugs at the intracellular level[28]. We evaluated different drug combinations to optimize the drug ratio of DTX-DCMs and BTZ-DCMs. Among all the pre-selected drug ratios, the IC_{50} was the lowest when the ratio of DTX-DCMs:BTZ-DCMs was 1:1.

In vitro anti-tumor activities of the nanoformulations

The *in vitro* cytotoxicity of free drug, blank DCMs (nanocarrier) and drug-loaded DCMs was evaluated in KYSE30 cells by the MTT assay. As shown in Figure 7A, the cell killing between the groups of free DTX and DTX-DCMs was similar, and the IC_{50} concentration was 43.26 μg/mL in the DTX group and 49.65 μg/mL in the DTX-DCMs group. The cell viability decreased sharply in the concentration range of 32 to 64 μg/mL, and the cell survival rate was relatively stable in the concentration range of 0.5 to 32 μg/mL. For BTZ, the IC_{50} concentration was 25.13 μg/mL in the BTZ group and 25.09 μg/mL in the BTZ-DCMs group. The cell viability decreased dramatically in the concentration range of 0.7 to 64 μg/mL. Furthermore, the cell viability data indicated that there was no obvious toxicity of blank DCMs (Figure 7A).

To investigate the synergistic effect of the two nanoformulations, KYSE30 cells were treated with DTX-DCMs and BTZ-DCMs concurrently (named as DTX-DCMs+BTZ-DCMs) and sequentially (DTX-DCMs followed by BTZ-DCMs (named as DTX-DCMs/BTZ-DCMs) and BTZ-DCMs followed by DTX-DCMs (named as BTZ-DCMs/DTX-DCMs). The cell viability was evaluated by the MTT assay. The results in Figure 7B and 7C revealed that treatment of KYSE30 cells with the combination of DTX-DCMs and BTZ-DCMs led to significant increases in apoptosis and induction of cell death compared to DTX-DCMs or BTZ-DCMs alone, indicating that they have a synergistic effect on esophageal cancer cells. Furthermore, the sequential treatment with DTX-DCMs followed by BTZ-DCMs was more effective than concurrent treatment (DTX-DCMs+BTZ-DCMs) and sequential treatment that was administered in a different order (BTZ-DCMs/DTX-DCMs). Determined by means of variance analysis (Figure 7C), the concentrations from 1.56 to 25 μg/mL were all statistically significant ($P<0.05$), which further confirmed that the best anti-

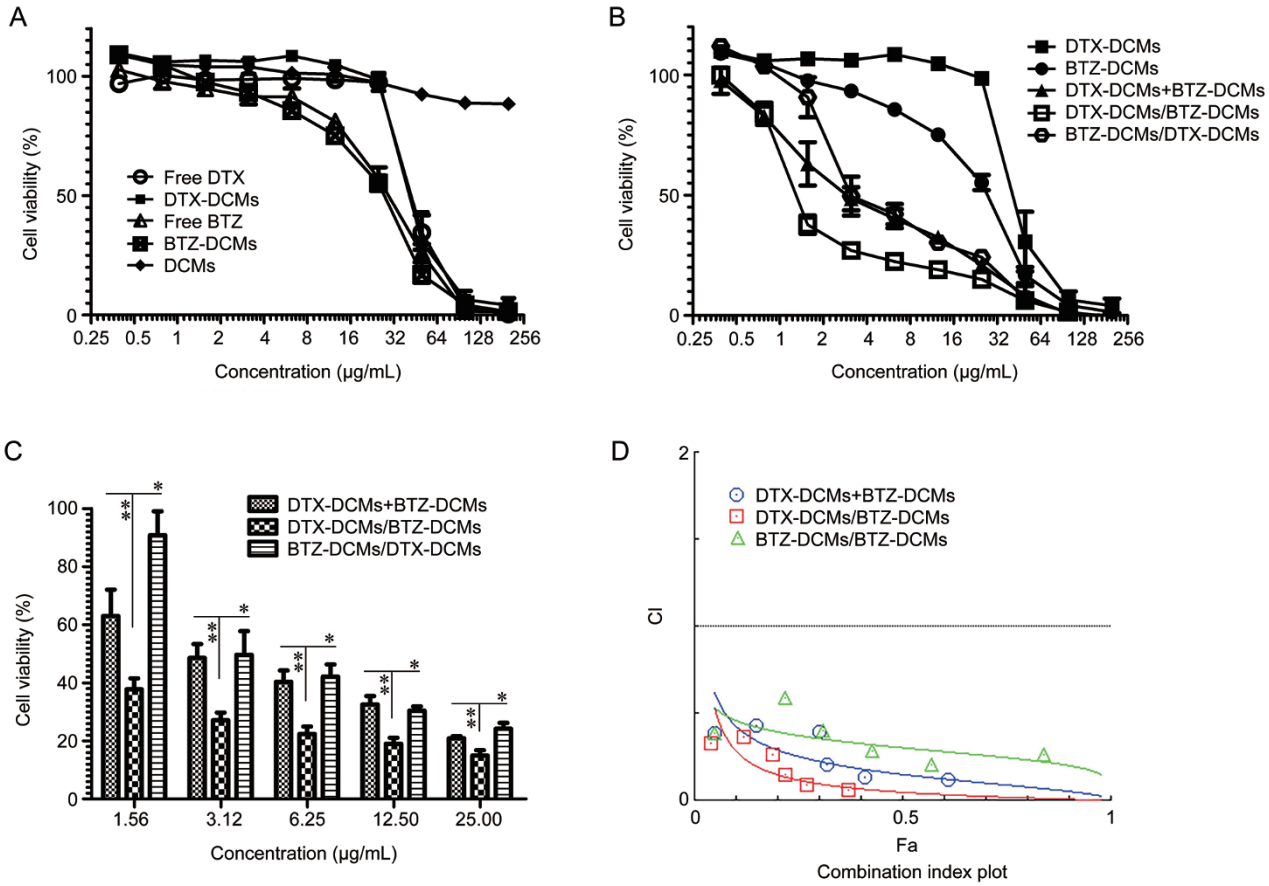

Figure 7. Anti-tumor activity and cytotoxicity of DTX-DCMs and BTZ-DCMs in KYSE30 cells and a combination index plot. MTT assays showing the viability of KYSE30 cells after 48 h of incubation with different concentrations of free drug, blank DCMs and drug-DCMs. The DTX-DCMs+BTZ-DCMs denotes that BTZ-DCMs and DTX-DCMs are concurrently combined. DTX-DCMs/BTZ-DCMs denotes that BTZ-DCMs were sequentially followed with DTX/DCMs, and the opposite sequential order is denoted by BTZ-DCMs/DTX-DCMs. (A) MTT assay results of free drug, blank DCMs and drug-DCMs. (B) MTT assay result of DTX-DCMs, BTZ-DCMs and DTX-DCMs with BTZ-DCMs (concurrently or sequentially). (C) Histogram of DTX-DCMs with BTZ-DCMs (concurrently or sequentially). Variance analysis was used in the comparison group, and it was all statistically significant at concentrations that ranged from 1.56 to 25 μg/mL ($P<0.05$). (D) The combination index plots of DTX-DCMs with BTZ-DCMs (concurrently or sequentially). The CI values of these three agents were mostly less than 0.5, which indicates that there is a synergistic effect between DTX-DCMs and BTZ-DCMs.

tumor activity was achieved with the sequential treatment of DTX-DCMs/BTZ-DCMs. To further investigate whether DTX-DCMs and BTZ-DCMs had a synergistic effect, we analyzed combination indexes (CI) using CompuSyn software 1.0. The CI values of DTX-DCMs and BTZ-DCMs (concurrently and sequentially) are exhibited in Table 1 and Figure 7D. It was revealed that most CI values were less than 0.5, except for the BTZ-DCMs/DTX-DCMs group, which had a concentration of 50.00 μg/mL. Most importantly, when the concentrations were less than 25.00 μg/mL, the CI values of the DTX-DCMs/BTZ-DCMs were all less than 0.3, which strongly indicated that there is a synergistic effect between DTX-DCMs and BTZ-DCMs against KYSE30 cells.

Table 1. The CI values of DTX-DCMs with BTZ-DCMs (concurrently or sequentially).

Total dose (μg/mL)	CI value		
	DTX-DCMs+ BTZ-DCMs	DTX-DCMs/ BTZ-DCMs	BTZ-DCMs/ DTX-DCMs
100.000	0.38410	0.32832	0.38410
50.000	0.43294	0.36407	0.59334
25.000	0.39302	0.26210	0.40568
12.500	0.20926	0.14833	0.28740
6.250	0.13598	0.08899	0.20994
3.125	0.11732	0.06720	0.26497

Discussion

The main factor that hinders the application of anti-cancer drugs is the dose-limiting toxicity. Due to the lack of selectivity, high doses of anti-cancer drugs were administered to reach an effective blood concentration. However, high drug concentrations result in severe side effects in patients. Moreover, drug bioavailability is low. To overcome the above problems,

anti-cancer drugs can be loaded into nanocarriers. Nanoscale drug delivery systems have been investigated due to their effective protection against drug resistance, their targeted delivery of drugs, improvements in their therapeutic indexes, and reduced adverse effects[35–37]. To date, only a very limited number of nanomedicines have been approved for clinical use, such as albumin-bound paclitaxel[38], non-PEGylated liposomal doxorubicin[39] and polymeric micelle-formulated paclitaxel[40].

An ideal nanocarrier should have a high drug loading efficiency for many drugs, a relatively small particle size (10–100 nm), low toxicity, good stability, controlled release and excellent tumor-targeting capabilities[41-43]. Based on these criteria, we chose disulfide cross-linked micelles as a versatile nanoplatform to formulate the anti-cancer drugs DTX and BTZ. We showed the size of DTX-DCMs and BTZ-DCMs to be 22.4±9 nm and 20.6±8 nm, respectively. Furthermore, the entrapment efficiency of both DTX and BTZ in DCMs was greater than 80%.

Through analysis of cell apoptosis and the cell cycle, the mechanisms underlying DTX-DCMs-mediated cell death were further explored in the KYSE30 human esophageal cancer cell line. Our data suggested that multiple mechanisms were potentially involved. We found that DTX-DCMs significantly induced apoptosis, and the biological factor that induced apoptosis was drug-induced cell cycle arrest in the G_2 phase. To further explore the potential molecular mechanism and signaling pathway of DTX-DCMs-mediated cell death, we analyzed some proteins related to apoptosis. Based on Western blot analysis, we hypothesized that p-ERK/PKCε/ NF-κB may be the signaling pathway involved. Boutros *et al*[44] demonstrates that ERK activation is involved in several functions, including cell proliferation. Chauvin *et al*[45] reported that the DTX-induced activation of the ERK signaling pathway can increase PKCε activity by 30% and the phosphatidic acid level by 1.6-fold. In addition, the activity of PKCε was positively correlated with phosphorylated ERK1/2 levels[46]. Nuclear factor κB (NF-κB) is an ubiquitously distributed transcription factor that controls the expression of genes involved in the cell cycle, immune responses, cell and tissue differentiation, and DNA repair[47]. NF-κB activation has proven to be an important signaling pathway in the occurrence and development of many kinds of tumors. An earlier report showed that the tumor suppressor function of NF-κB was mediated by down-regulating protein phosphatase 1a, which leads to the preservation of phosphorylation on p-ERK and inhibition of the apoptotic pathway[48]. In our present study, we presumed that the p-ERK/PKCε/NF-κB pathway might be a latent signaling pathway during cancer cell treatment with DTX. Further studies are warranted to investigate this in detail. Furthermore, we used cell cycle analysis to confirm that BTZ was not the drug that induced apoptosis by inhibiting differentiation. Using Western blot analysis, we demonstrated that BTZ activated the intrinsic pathway by down-regulating p38 and anti-apoptotic proteins, such as Bcl-2. The activation of Bcl-2 may increase MMP and activate caspase-3, and increased levels of cleaved caspase-3 are reliable indicators of apoptosis[30]. Thus, we suggest that p38/NF-κB/Bcl-2 may be the potential signaling pathway that induces apoptosis. Interestingly, Western blot analysis demonstrated that the level of PKCε protein was slightly changed, but p-ERK was obviously up-regulated following BTZ treatment, indicating that BTZ and DTX may have a synergistic effect.

We systemically investigated the impact of the sequence and the drug ratio of the combination therapies on *in vitro* antitumor activities. Our data from the MTT assays demonstrated that the most effective method was using a 1:1 ratio of DTX-DCMs and BTZ-DCMs in sequential treatment (DTX-DCMs/BTZ-DCMs). The data were statistically significant in concentrations ranging from 1.56 to 25 μg/mL ($P<0.05$) compared with the other treatments. Furthermore, we analyzed the combination indexes through CompuSyn software 1.0. Based on the CI plot and the CI values of DTX-DCMs and BTZ-DCMs, we concluded that there was a synergistic effect between DTX-DCMs and BTZ-DCMs, particularly when DTX-DCMs were applied prior to BTZ-DCMs. This result is consistent with previous preclinical studies in prostate and lung cancer models[19]. These findings suggest an immense potential for the sequential treatment method (DTX-DCMs/BTZ-DCMs) in clinical applications to improve the therapeutic responses to DTX and BTZ.

In summary, we have successfully developed nanoformulations of DTX and BTZ by utilizing disulfide cross-linked micelles. These DTX- and BTZ-loaded nanoparticles were relatively small in diameter and exhibited a high drug loading efficiency. These nanodrugs could be effectively internalized by human esophageal cancer cells, and they played a significant role in cell apoptosis. Furthermore, there was a strong synergistic effect between DTX-DCMs and BTZ-DCMs against an esophageal cancer cell line. Sequential combination therapy with DTX-DCMs followed by BTZ-DCMs showed the best *in vitro* anti-tumor efficacy. *In vivo* therapeutic and toxicity studies are currently underway to further evaluate DTX-DCMs and BTZ-DCMs in esophageal cancer animal models. The nanoformulations of DTX and BTZ showed great promise; therefore, further investigations of combination therapy to improve the treatment efficacy of esophageal cancer are warranted.

Acknowledgements

This work was financially supported by NIH/NCI (R01CA199668) and NIH/NICHD (R01HD086195).

References

1 Siegel RL, Miller KD, Jemal A. Cancer statistics, 2016. CA Cancer J Clin 2016; 66: 7–30.
2 Chen W, Zheng R, Baade PD, Zhang S, Zeng H, Bray F, *et al*. Cancer statistics in China, 2015. CA Cancer J Clin 2016; 66: 115–32.
3 Collins DC, Sundar R, Lim JS, Yap TA. Towards precision medicine in the clinic: From biomarker discovery to novel therapeutics. Trends Pharmacol Sci 2017; 38: 25–40.
4 Tan Q, Liu X, Fu X, Li Q, Dou J, Zhai G. Current development in nanoformulations of docetaxel. Expert Opin Drug Deliv 2012; 9: 975–90.
5 Fushida S, Nashimoto A, Fukushima N, Kawachi Y, Fujimura T,

Kuwabara S, *et al*. Phase II trial of preoperative chemotherapy with docetaxel, cisplatin and S-1 for T4 locally advanced gastric cancer. Jpn J Clin Oncol 2012; 42: 131–3.
6 Fei F, Chen C, Xue J, Di GH, Lu JS, Liu GY, *et al*. Efficacy and safety of docetaxel combined with oxaliplatin as a neoadjuvant chemotherapy regimen for Chinese triple-negative local advanced breast cancer patients. A prospective, open, and unicentric Phase II clinical trial. Am J Clin Oncol 2013; 36: 545–51.
7 Francis P, Schneider J, Hann L, Balmaceda C, Barakat R, Phillips M, *et al*. Phase II trial of docetaxel in patients with platinum-refractory advanced ovarian cancer. J Clin Oncol 1994; 12: 2301–8.
8 Hironaka S, Tsubosa Y, Mizusawa J, Kii T, Kato K, Tsushima T, *et al*. Phase I/II trial of 2-weekly docetaxel combined with cisplatin plus fluorouracil in metastatic esophageal cancer (JCOG0807). Cancer Sci 2014; 105: 1189–95.
9 Des Guetz G, Landre T, Westeel V, Milleron B, Vaylet F, Urban T, *et al*. Similar survival rates with first-line gefitinib, gemcitabine, or docetaxel in a randomized phase II trial in elderly patients with advanced non-small cell lung cancer and a poor performance status (IFCT-0301). J Geriatr Oncol 2015; 6: 233–40.
10 Baker SD, Sparreboom A, Verweij J. Clinical pharmacokinetics of docetaxel: recent developments. Clin Pharmacokinet 2006; 45: 235–52.
11 Clarke SJ, Rivory LP. Clinical pharmacokinetics of docetaxel. Clin Pharmacokinet 1999; 36: 99–114.
12 Hideshima T, Richardson P, Chauhan D, Palombella VJ, Elliott PJ, Adams J, *et al*. The proteasome inhibitor PS-341 inhibits growth, induces apoptosis, and overcomes drug resistance in human multiple myeloma cells. Cancer Res 2001; 61: 3071–6.
13 You SA, Basu A, Haldar S. Potent antitumor agent proteasome inhibitors: a novel trigger for Bcl2 phosphorylation to induce apoptosis. Int J Oncol 1999; 15: 625–8.
14 Ocean AJ, Christos P, Sparano JA, Shah MA, Yantiss RK, Cheng J, *et al*. Phase II trial of bortezomib alone or in combination with irinotecan in patients with adenocarcinoma of the gastroesophageal junction or stomach. Invest New Drugs 2014; 32: 542–8.
15 Nawrocki ST, Sweeney-Gotsch B, Takamori R, McConkey DJ. The proteasome inhibitor bortezomib enhances the activity of docetaxel in orthotopic human pancreatic tumor xenografts. Mol Cancer Ther 2004; 3: 59–70.
16 Canfield SE, Zhu K, Williams SA, McConkey DJ. Bortezomib inhibits docetaxel-induced apoptosis via a p21-dependent mechanism in human prostate cancer cells. Mol Cancer Ther 2006; 5: 2043–50.
17 Chung CH, Aulino J, Muldowney NJ, Hatakeyama H, Baumann J, Burkey B, *et al*. Nuclear factor-kappa B pathway and response in a phase II trial of bortezomib and docetaxel in patients with recurrent and/or metastatic head and neck squamous cell carcinoma. Ann Oncol 2010; 21: 864–70.
18 Lara PN Jr, Longmate J, Reckamp K, Gitlitz B, Argiris A, Ramalingam S, *et al*. Randomized phase II trial of concurrent versus sequential bortezomib plus docetaxel in advanced non-small-cell lung cancer: a California cancer consortium trial. Clin Lung Cancer 2011; 12: 33–7.
19 Awada A, Albanell J, Canney PA, Dirix LY, Gil T, Cardoso F, *et al*. Bortezomib/docetaxel combination therapy in patients with anthracycline-pretreated advanced/metastatic breast cancer: a phase I/II dose-escalation study. Br J Cancer 2008; 98: 1500–7.
20 Zhang M, Wei W, Liu J, Yang H, Jiang Y, Tang W, *et al*. Comparison of the effectiveness and toxicity of neoadjuvant chemotherapy regimens, capecitabine/epirubicin/cyclophosphamide *vs* 5-fluorouracil/epirubicin/cyclophosphamide, followed by adjuvant, capecitabine/docetaxel *vs* docetaxel, in patients with operable breast cancer. Onco Targets Ther 2016; 9: 3443–50.
21 Schweizer MT, Gulati R, Mostaghel EA, Nelson PS, Montgomery RB, Yu EY, *et al*. Docetaxel-related toxicity in metastatic hormone-sensitive and metastatic castration-resistant prostate cancer. Med Oncol 2016; 33: 77.
22 Bruchim I, Weeg N, Alpert Y, Sade D, Piura E, Fishman A. High efficacy and low toxicity of the modified docetaxel and carboplatin protocol in patients with recurrent ovarian cancer-a phase 2 cohort study. Int J Gynecol Cancer 2016; 26: 640–7.
23 Chanat C, Delbaldo C, Denis J, Bocaccio F, Cojean-Zelek I, Le Guyader N. Dose intensity and toxicity associated with Taxotere formulation: a retrospective study in a population of breast cancer patients treated with docetaxel as an adjuvant or neoadjuvant chemotherapy. Anti-cancer Drugs 2015; 26: 984–9.
24 Senapati PC, Sahoo SK, Sahu AN. Mixed surfactant based (SNEDDS) self-nanoemulsifying drug delivery system presenting efavirenz for enhancement of oral bioavailability. Biomed Pharmacother 2016; 80: 42–51.
25 Gao Y, Shen JK, Choy E, Zhang Z, Mankin HJ, Hornicek FJ, *et al*. Pharmacokinetics and tolerability of NSC23925b, a novel P-glycoprotein inhibitor: preclinical study in mice and rats. Sci Rep 2016; 6: 25659.
26 Koo AN, Lee HJ, Kim SE, Chang JH, Park C, Kim C, *et al*. Disulfide-cross-linked PEG-poly(amino acid)s copolymer micelles for glutathione-mediated intracellular drug delivery. Chem Commun (Camb) 2008; (48): 6570–2.
27 Yu S, Ding J, He C, Cao Y, Xu W, Chen X. Disulfide cross-linked polyurethane micelles as a reduction-triggered drug delivery system for cancer therapy. Adv Healthc Mater 2014; 3: 752–60.
28 Li Y, Xiao K, Luo J, Xiao W, Lee JS, Gonik AM, *et al*. Well-defined, reversible disulfide cross-linked micelles for on-demand paclitaxel delivery. Biomaterials 2011; 32: 6633–45.
29 Ho MY, Mackey JR. Presentation and management of docetaxel-related adverse effects in patients with breast cancer. Cancer Manag Res 2014; 6: 253–9.
30 Xiao K, Li YP, Wang C, Ahmad S, Vu M, Kuma K, *et al*. Disulfide cross-linked micelles of novel HDAC inhibitor thailandepsin A for the treatment of breast cancer. Biomaterials 2015; 67: 183–93.
31 Vysloužil J, Bavoľárová J, Kejdušová M, Vetchý D, Dvořáčková K. Cationic Eudragit® polymers as excipients for microparticles prepared by solvent evaporation method. Ceska Slov Farm 2013; 62: 249–54.
32 Luo J, Xiao K, Li Y, Lee JS, Shi L, Tan YH, *et al*. Well-defined, size-tunable, multifunctional micelles for efficient paclitaxel delivery for cancer treatment. Bioconjug Chem 2010; 21: 1216–24.
33 Xiao K, Luo J, Fowler WL, Li Y, Lee JS, Xing L, *et al*. A self-assembling nanoparticle for paclitaxel delivery in ovarian cancer. Biomaterials 2009; 30: 6006–16.
34 Xiao K, Luo J, Li Y, Lee J S, Fung G, Lam KS. PEG-oligocholic acid telodendrimer micelles for the targeted delivery of doxorubicin to B-cell lymphoma. J Control Release 2011; 155: 272–81.
35 Wei X, Luo Q, Sun L, Li X, Zhu H, Guan P, *et al*. Enzyme- and pH-sensitive branched polymer-doxorubicin conjugate-based nanoscale drug delivery system for cancer therapy. ACS Appl Mater Interfaces 2016; 8: 11765–78.
36 An J, Dai X, Wu Z, Zhao Y, Lu Z, Guo Q, *et al*. An acid-triggered degradable and fluorescent nanoscale drug delivery system with enhanced cytotoxicity to cancer cells. Biomacromolecules 2015; 16: 2444–54.
37 Brown PK, Qureshi AT, Moll AN, Hayes DJ, Monroe WT. Silver nanoscale antisense drug delivery system for photoactivated gene silencing. ACS Nano 2013; 7: 2948–59.

38 Yoshida H, Kim YH, Ozasa H, Nagai H, Sakamori Y, Nakaoku T, *et al*. Albumin-bound paclitaxel for the treatment of refractory or relapsed small-cell lung cancer. Mol Clin Oncol 2016; 5: 213–5.
39 Rohlfing S, Aurich M, Schöning T, Ho AD, Witzens-Harig M. Non-pegylated liposomal doxorubicin as a component of R-CHOP is an effective and safe alternative to conventional doxorubicin in the treatment of patients with diffuse large B-Cell lymphoma and preexisting cardiac diseases. Clin Lymphoma Myeloma Leuk 2015; 15: 458–63.
40 Park IH, Sohn JH, Kim SB, Lee KS, Chung JS, Lee SH, *et al*. An open-label, randomized, parallel, phase III trial evaluating the efficacy and safety of polymeric micelle-formulated paclitaxel compared to conventional cremophor EL-based paclitaxel for recurrent or metastatic HER2-negative breast cancer. Cancer Res Treat 2016. doi: 10.4143/crt.2016.289.
41 Yokoyama M. Drug targeting with nano-sized carrier systems. J Artif Organs 2005; 8: 77–84.
42 Xiong F, Tian J, Hu K, Zheng X, Sun J, Yan C, *et al*. Superparamagnetic anisotropic nano-assemblies with longer blood circulation *in vivo*: a highly efficient drug delivery carrier for leukemia therapy. Nanoscale 2016; 8: 17085–9.
43 Kohli AK, Alpar HO. Potential use of nanoparticles for transcutaneous vaccine delivery: effect of particle size and charge. Int J Pharm 2004; 275: 13–7.
44 Boutros T, Chevet E, Metrakos P. Mitogen-activated protein (MAP) kinase/MAP kinase phosphatase regulation: roles in cell growth, death, and cancer. Pharmacol Rev 2008; 60: 261–310.
45 Chauvin L, Goupille C, Blanc C, Pinault M, Domingo I, Guimaraes C, *et al*. Long chain n-3 polyunsaturated fatty acids increase the efficacy of docetaxel in mammary cancer cells by downregulating Akt and PKCε/δ-induced ERK pathways. Biochim Biophys Acta 2016; 1861: 380–90.
46 McDaid HM, Lopez-Barcons L, Grossman A, Lia M, Keller S, Pérez-Soler R, *et al*. Enhancement of the therapeutic efficacy of taxol by the mitogen-activated protein kinase kinase inhibitor CI-1040 in nude mice bearing human heterotransplants. Cancer Res 2005; 65: 2854–60.
47 Panday A, Inda ME, Bagam P, Sahoo MK, Osorio D, Batra S. Transcription factor NF-κB: an update on intervention strategies. Arch Immunol Ther Exp (Warsz) 2016; 64: 463–83.
48 Yang G, Xiao X, Rosen DG, Cheng X, Wu X, Chang B, *et al*. The biphasic role of NF-kappaB in progression and chemoresistance of ovarian cancer. Clin Cancer Res 2011; 17: 2181–94.